



Size effect and dynamic properties of 2D lattice materials



Geminiano Mancusi^{a, *}, Francesco Fabbrocino^b, Luciano Feo^a, Fernando Fraternali^a

^a Department of Civil Engineering, University of Salerno, Fisciano, Italy

^b Telematic University "Pegaso", Naples, Italy

ARTICLE INFO

Article history:

Received 8 November 2016

Received in revised form

8 November 2016

Accepted 7 December 2016

Available online 18 December 2016

Keywords:

Periodic materials

2D lattices

Band gaps

Microstructure

FEM

ABSTRACT

The dynamic analysis of two-dimensional (2D) periodic material structures is proposed via a novel mechanical approach. General assumptions include: i) the representative unit cell of the square lattice can be modeled by means of a defined number of straight micro-beams; ii) both shear/flexural and axial strains are locally accounted for; iii) a microstructure-dependent scale length is introduced as an intrinsic parameter of the micro-beams, with possible different scale lengths for different considered beams. All these features allow to detect the influence of the characteristics of the lattice at the local scale on the global dynamic behavior. Moreover, the existence of frequency band gaps is also predicted.

© 2016 Elsevier Ltd. All rights reserved.

1. Introduction

The research and development of micro-structured periodic materials have revealed a great appeal over the last years, in view of the numerous advantages related to them. The enhanced structural performances, in fact, include the high strength to weight and stiffness to weight ratios as well as specific dynamic properties [1–6]. Photonic and phononic crystals, energy absorption devices, noise and vibration controllers as well as advanced strategies for the seismic isolation, in fact, are fields of investigation open to new contributions [7–12]. Within this context, a relevant position is taken by 2D lattice materials.

As discussed by many authors, the dynamic behavior of a square lattice material is strongly affected by the underlying microstructure. Where changes in stresses and strains can no longer be considered as uniform at the local scale, the importance of considering a microstructure-dependent parameter becomes imperative [13–16]. A similar situation deals, for example, with thin films, adhesive interfaces, notches, crack tips, localized deformations.

Several simplifications are usually introduced when studying the dynamic response of periodic materials. First of all, the spatial periodicity (i.e. the hypothesis of infinite lattice points) allows to

reduce the analysis to the representative unit cell (RUC), by means of the Bloch theorem. An example of a simple two-dimensional square lattice material and the corresponding unit cell is depicted in Fig. 1, where \mathbf{a}_1 and \mathbf{a}_2 are the unit vectors along the directions of spatial periodicity. The square topology implies, in this case, that \mathbf{a}_1 and \mathbf{a}_2 are normal to each other.

According to the Bloch theorem, if a plane elastic wave propagates in the lattice material (Fig. 1), the displacement of an arbitrary point \mathbf{P} is given by:

$$\mathbf{u}(\mathbf{r}) = \mathbf{u}_k(\mathbf{r}) \exp(-i\omega t + \mathbf{k} \cdot \mathbf{r}) \quad (1)$$

with the symbol \mathbf{r} indicating the position of the point \mathbf{P} , \mathbf{k} denoting the Bloch wave vector, ω the angular frequency and the amplitude $\mathbf{u}_k(\mathbf{r})$ being characterized by the same spatial periodicity as the point lattice. By virtue of this, the position of an arbitrary point \mathbf{P} at a fixed time t is a function of the position of the corresponding point \mathbf{O} , which is located in a reference unit cell. Once the reference cell has been fixed (see Fig. 1), it results: $\mathbf{r} = \mathbf{r}_0 + n_1 \mathbf{a}_1 + n_2 \mathbf{a}_2$ where (n_1, n_2) is an integer pair, \mathbf{a}_1 and \mathbf{a}_2 the generating vectors and \mathbf{r}_0 is the position vector of \mathbf{O} . Equation (1) becomes:

$$\mathbf{u}(\mathbf{r}) = \mathbf{u}(\mathbf{r}_0) \exp(n_1 \mathbf{k} \cdot \mathbf{a}_1 + n_2 \mathbf{k} \cdot \mathbf{a}_2) \quad (2)$$

By other words, it is possible to restrict the study of an infinite lattice system to the analysis of the reference unit cell, which is also called representative unit cell (RUC).

It is easy to verify that the reciprocal unit vectors \mathbf{b}_1 and \mathbf{b}_2

* Corresponding author.

E-mail address: g.mancusi@unisa.it (G. Mancusi).

Notation			
Ω	global reference system (origin)	l_1	length of the primary micro-beams ($l_1 = a/2$)
$\mathbf{e}_1, \mathbf{e}_2, \mathbf{e}_3$	global reference system (unit vectors)	l_2	length of the auxiliary micro-beams ($l_2 \leq a\sqrt{2}/2$)
a	lattice constant	A	cross-section area (per unit length along \mathbf{e}_3)
$\mathbf{a}_1, \mathbf{a}_2$	generating vectors ($\mathbf{a}_i = a\mathbf{e}_i$ with $i = 1, 2$)	A_s	cross-section shear area (per unit length along \mathbf{e}_3)
$\mathbf{b}_1, \mathbf{b}_2$	reciprocal unit vectors	I	flexural inertia (per unit length along \mathbf{e}_3)
$\mathbf{i}_1, \mathbf{i}_2, \mathbf{i}_3$	local reference system (unit vectors) - \mathbf{i}_1 aligned with the beam axis	E	longitudinal normal modulus
\mathbf{k}	Bloch wave vector	G	shear modulus
\mathbf{E}	symmetric part of the displacement gradient	ν	Poisson ratio
κ	symmetric part of the curvature tensor	l	microscale characteristic length
\mathbf{S}	Cauchy stress tensor	ρ	mass density
\mathbf{M}	couple stress tensor	N	axial force
$\bar{\mathbf{m}}$	deviatoric part of \mathbf{M}	M	bending moment
		Y	additional bending moment depending on the size effect
		V	shear force

assume the following form:

$$\mathbf{b}_1 = 2\pi \frac{\mathbf{a}_2 \times \mathbf{e}_3}{\mathbf{a}_1 \cdot (\mathbf{a}_2 \times \mathbf{e}_3)} = \frac{2\pi}{a} \mathbf{e}_1 \tag{3.1}$$

$$\mathbf{b}_2 = 2\pi \frac{\mathbf{e}_3 \times \mathbf{a}_1}{\mathbf{a}_1 \cdot (\mathbf{a}_2 \times \mathbf{e}_3)} = \frac{2\pi}{a} \mathbf{e}_2 \tag{3.2}$$

where \mathbf{e}_3 is the unit vector normal to the $\mathbf{e}_1 - \mathbf{e}_2$ plane (Fig. 1).

Finally, the periodic boundary condition for the dynamic analysis of the unit cell assumes the following form:

$$\mathbf{u}(\mathbf{r}) = \mathbf{u}(\mathbf{r}_0) \exp[2\pi(n_1 k_1 + n_2 k_2)] \tag{4}$$

under the hypothesis the Bloch wave vector is expressed in the reciprocal space:

$$\mathbf{k} = k_1 \mathbf{b}_1 + k_2 \mathbf{b}_2 \tag{5}$$

2. Mechanical approach

The mechanical model proposed for the dynamic analysis of a 2D lattice material is discussed in this section. The following assumptions are made:

- i) The spatial periodicity directions \mathbf{a}_1 and \mathbf{a}_2 are orthogonal to each other;

- ii) The representative unit cell can be simulated by inter-connecting straight micro-beams (Fig. 2);
- iii) The primary microstructure is made of four micro-beams, which are always present. Auxiliary micro-beams can be present depending on the designed topology;
- iv) Rigid internal connections are considered;
- v) An appropriate micro-scale parameter is introduced in order to simulate the local behavior of a generic micro-beam, thus accounting for the so-called size effect [17–19].

Examples of RUCs are shown in Fig. 2. The first example (left side) shows the presence of the main micro-structures, made of four primary micro-beams only. The second example (right side) indicates that auxiliary micro-beams can be present in addition to the main micro-structures. It is worth noting auxiliary micro-beams are directly related to the resonance properties at the local scale of the periodic material.

In order to account for the micro-beams local behavior, couple stresses are considered in addition to classical Cauchy stresses. The deformation energy density, w , has been thereby assumed as follows, in accordance with [17,18]:

$$w = \frac{1}{2} \lambda (\text{tr} \mathbf{E})^2 + \mu (\mathbf{E} \cdot \mathbf{E} + l^2 \kappa \cdot \kappa) \tag{6}$$

where λ and μ denote the Lamé's constants, while l is a micro-structure length scale parameter. With usual notation, \mathbf{E} and κ indicate, respectively, the symmetric part of the displacement gradient and the symmetric part of the curvature tensor:

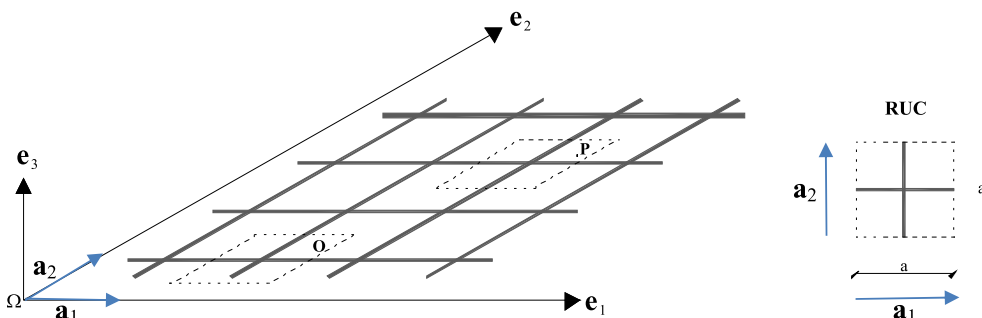


Fig. 1. Two-dimensional square lattice material (example).

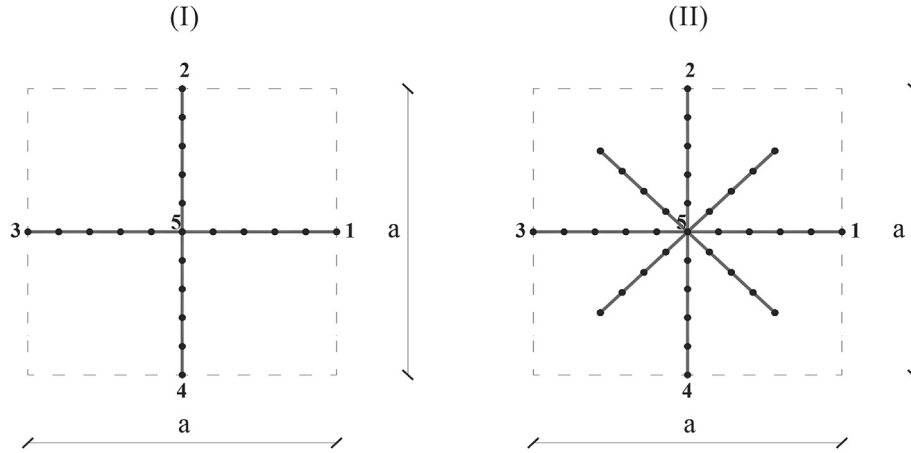


Fig. 2. Examples of RUCs of a 2D square lattice material (a being the lattice constant).

$$E_{ij} = 1/2 [\partial u_i / \partial x_j + \partial u_j / \partial x_i] \tag{7.1}$$

$$\kappa_{ij} = 1/2 (\partial \theta_i / \partial x_j + \partial \theta_j / \partial x_i) \tag{7.2}$$

It is important to remark that the strain tensor \mathbf{E} is conjugated with the Cauchy stresses, \mathbf{S} , while κ is conjugated with the deviatoric part, $\overline{\mathbf{m}}$, of the couple stress tensor \mathbf{M} . It is also important to underline that couple stresses are considered in a simplified manner, according to the so-called Modified Couple Stress Theory [17,18], which, as demonstrated in Ref. [20], has been built up on the assumption that only the symmetric part of the rotation gradient contributes to the strain energy density, while the skew-symmetric part does not influence the behavior of the beam.

With reference to a generic micro-beam of the RUC, the displacement field can be assumed as follows:

$$u_1 = u(x) - \varphi(x)y, \tag{8.1}$$

$$u_2 = v(x), \tag{8.2}$$

$$u_3 = 0. \tag{8.3}$$

where u_1 , u_2 and u_3 are the displacement field components along the local axes ($\mathbf{i}_1, \mathbf{i}_2, \mathbf{i}_3$) with \mathbf{i}_1 coinciding with the axis of the beam; x and y denoting the rectangular coordinates referred to \mathbf{i}_1 and \mathbf{i}_2 , respectively; $u(x)$ and $v(x)$ being the translational components of the cross-section displacement while $\varphi(x) = \theta_3(x)$ the

Table 1
Geometry and mechanical parameters (I/II indicates the considered topology of the RUC as in Fig. 2).

#	RUC	a [mm]	l_1 [mm]	A [mm ² /mm]	A_s [mm ² /mm]	I [mm ⁴ /mm]	l_2 [mm]	E [N/mm ²]	ν	G [N/mm ²]	ρ [kg/mm ³]
1	I	1.0×10^{-1}	5.0×10^{-2}	5.0×10^{-3}	4.17×10^{-3}	1.04×10^{-8}	0.00	9.0×10^4	0.23	3.66×10^4	2.70×10^{-6}
2	II	1.0×10^{-1}	5.0×10^{-2}	5.0×10^{-3}	4.17×10^{-3}	1.04×10^{-8}	3.54×10^{-2}	9.0×10^4	0.23	3.66×10^4	2.70×10^{-6}
3	I	1.0×10^{-1}	5.0×10^{-2}	1.0×10^{-2}	8.33×10^{-3}	8.33×10^{-8}	0.00	9.0×10^4	0.23	3.66×10^4	2.70×10^{-6}
4	II	1.0×10^{-1}	5.0×10^{-2}	1.0×10^{-2}	8.33×10^{-3}	8.33×10^{-8}	3.54×10^{-2}	9.0×10^4	0.23	3.66×10^4	2.70×10^{-6}
5	I	1.0×10^{-1}	5.0×10^{-2}	2.0×10^{-2}	1.67×10^{-2}	6.67×10^{-7}	0.00	9.0×10^4	0.23	3.66×10^4	2.70×10^{-6}
6	II	1.0×10^{-1}	5.0×10^{-2}	2.0×10^{-2}	1.67×10^{-2}	6.67×10^{-7}	3.54×10^{-2}	9.0×10^4	0.23	3.66×10^4	2.70×10^{-6}

Table 2
First natural frequencies ω_1 at points O, A, B (1.a, 1.b, 2.a, 2.b and 2.c).

		1	2	3	4	5	6	7	8	9	10
1.a	O	0.0	0.0	4.2	4.2	6.1	9.3	18.8	18.8	23.9	29.4
	A	0.8	2.4	3.3	7.0	11.5	13.2	14.5	20.0	25.5	32.9
	B	1.7	2.2	8.9	11.6	11.6	12.7	17.0	17.0	28.9	34.7
1.b	O	0.0	0.0	10.8	10.8	15.9	21.7	37.1	37.1	52.1	56.4
	A	2.0	6.6	7.5	15.9	17.8	25.7	30.4	36.6	51.6	53.2
	B	4.2	5.7	14.1	14.1	22.1	27.4	30.6	30.9	48.2	48.3
2.a	O	0.0	0.0	2.6	3.7	4.0	4.3	4.3	4.8	7.9	9.3
	A	0.6	2.2	3.0	3.3	4.2	4.3	4.3	8.4	10.3	11.9
	B	1.5	2.2	3.0	4.2	4.3	4.3	9.7	9.8	10.7	12.7
2.b	O	0.0	0.0	2.9	3.8	4.0	9.3	9.6	11.4	11.4	12.4
	A	0.6	2.2	3.3	3.5	8.4	9.5	11.4	11.4	12.7	13.5
	B	1.5	2.2	3.5	8.2	9.8	11.4	11.4	12.6	12.7	12.7
2.c	O	0.0	0.0	7.0	9.6	10.2	11.4	11.4	12.7	19.5	21.7
	A	1.5	6.0	6.8	8.0	10.1	11.4	11.4	14.5	20.4	26.4
	B	3.7	5.7	7.7	8.8	11.4	11.4	11.5	13.8	25.0	27.3

Table 3
First natural frequencies ω_1 at points **O, A, B** (3.a, 3.b, 4.a, 4.b and 4.c).

		1	2	3	4	5	6	7	8	9	10
3.a	O	0.0	0.0	4.0	4.0	5.8	8.3	15.4	15.4	20.4	23.3
	A	0.7	2.4	3.0	6.6	7.3	10.1	12.2	15.5	21.3	24.1
	B	1.6	2.1	6.7	6.7	8.2	10.9	12.6	12.6	22.6	22.7
3.b	O	0.0	0.0	6.0	6.0	8.9	11.7	19.4	19.4	27.7	29.4
	A	1.2	3.7	4.0	8.3	9.9	13.7	16.0	19.0	26.4	27.5
	B	2.3	3.2	7.2	7.2	12.1	14.5	16.0	16.2	24.5	24.5
4.a	O	0.0	0.0	2.5	3.5	3.8	4.1	4.1	4.6	7.3	8.3
	A	0.5	2.2	2.9	2.9	3.8	4.1	4.1	6.0	7.7	10.4
	B	1.4	2.1	2.8	3.7	4.1	4.1	5.3	5.7	9.6	10.9
4.b	O	0.0	0.2	2.7	3.6	3.8	6.4	6.4	7.0	8.1	8.3
	A	0.5	2.2	2.9	3.2	4.7	6.4	6.4	7.6	8.2	10.7
	B	1.4	2.1	3.1	4.4	5.4	6.4	6.4	7.4	10.4	10.9
4.c	O	0.0	0.2	4.0	5.3	5.7	6.4	6.4	7.1	10.7	11.7
	A	0.9	3.4	3.5	4.5	5.6	6.4	6.4	7.9	11.1	14.1
	B	2.0	3.2	4.3	4.7	6.0	6.4	6.4	7.5	13.5	14.5

Table 4
First natural frequencies ω_1 at points **O, A, B** (5.a, 5.b, 6.a, 6.b and 6.c).

		1	2	3	4	5	6	7	8	9	10
5.a	O	0.0	0.0	3.4	3.4	5.0	6.3	10.0	10.0	14.4	15.1
	A	0.7	2.1	2.1	4.3	5.4	7.2	8.2	9.7	13.4	13.9
	B	1.3	1.8	3.7	3.7	6.5	7.6	8.2	8.2	12.3	12.3
5.b	O	0.0	0.0	3.8	3.8	5.6	6.8	10.5	10.5	15.5	15.9
	A	0.8	2.2	2.4	4.6	6.1	7.7	8.7	10.1	13.8	14.4
	B	1.4	2.1	3.8	3.8	7.1	8.0	8.7	8.7	12.7	12.7
6.a	O	0.0	0.0	2.2	3.0	3.2	3.5	3.5	3.9	5.8	6.3
	A	0.5	1.8	1.9	2.5	3.1	3.5	3.5	4.3	6.0	7.4
	B	1.1	1.7	2.4	2.5	3.1	3.5	3.5	4.1	7.1	7.6
6.b	O	0.0	0.0	2.3	3.0	3.2	4.0	4.0	4.4	5.9	6.3
	A	0.5	1.8	1.9	2.6	3.2	4.0	4.0	4.7	6.1	7.4
	B	1.1	1.7	2.4	2.5	3.2	4.0	4.0	4.6	7.2	7.6
6.c	O	0.0	0.0	2.6	3.3	3.6	4.0	4.0	4.5	6.4	6.8
	A	0.6	1.9	2.2	2.9	3.5	4.0	4.0	4.8	6.6	7.9
	B	1.2	1.9	2.6	2.7	3.4	4.0	4.0	4.6	7.7	8.0

rotation referred to the $\mathbf{i}_3 = \mathbf{e}_3$ axis. For the considered problem (i.e. plane problem) the only non-trivial strain and curvature components are the following:

$$E_{11} = \frac{\partial u}{\partial x} - y \frac{\partial \varphi}{\partial x}, \tag{9.1}$$

$$E_{12} = E_{21} = \frac{1}{2} \left(\frac{\partial v}{\partial x} - \varphi \right), \tag{9.2}$$

$$\kappa_{13} = \kappa_{31} = \frac{1}{4} \left(\frac{\partial^2 v}{\partial x^2} + \frac{\partial \varphi}{\partial x} \right). \tag{9.3}$$

The generalized stresses of this beam model include the axial force (N), the bending moment (M), the additional bending moment related to the size-effect (Y) and the shear force (V). Finally, the following constitutive relationships exist:

$$[N, M, Y, V]^T = \mathbf{C} \left[\frac{\partial u}{\partial x}, \frac{\partial \varphi}{\partial x}, \frac{1}{2} \left(\frac{\partial \varphi}{\partial x} + \frac{\partial^2 v}{\partial x^2} \right), \left(-\varphi + \frac{\partial v}{\partial x} \right) \right]^T \tag{10}$$

where \mathbf{C} denotes the following matrix:

$$\mathbf{C} = \text{diag}(C_{11}, C_{22}, C_{33}, C_{44}) \tag{11}$$

with:

$$C_{11} = \frac{E(1-\nu)A}{(1+\nu)(1-2\nu)} \tag{12.1}$$

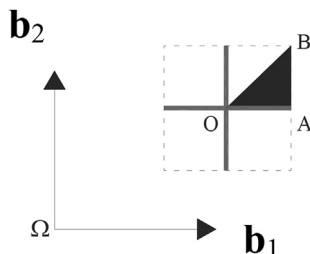


Fig. 3. Irreducible part of the first Brillouin zone.

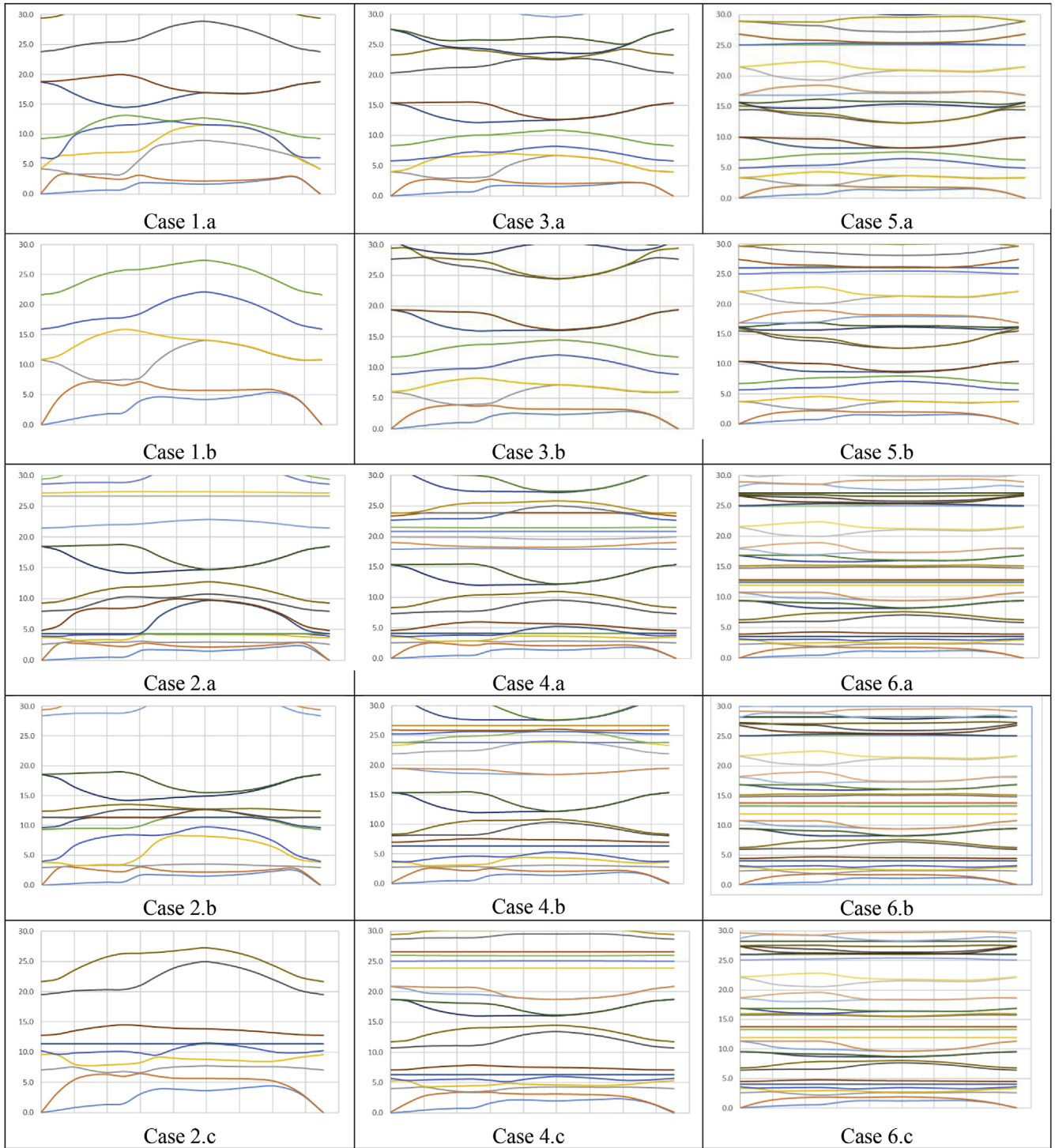


Fig. 4. Frequency band structures (not dimensional) (abscissa lying on the boundary **OABO** of the irreducible part of the first Brillouin zone).

$$C_{22} = \frac{E(1 - \nu)I}{(1 + \nu)(1 - 2\nu)} \tag{12.2}$$

$$C_{33} = GA_l^2 \tag{12.3}$$

$$C_{44} = GA_s \tag{12.4}$$

In previous eqs. (12.1,12.2,12.3,12.4) the symbols A , A_s and l denote the cross-section area, the cross-section area for shear and

the flexural inertia (per unit length), while the symbols E , G and ν denote the Young modulus, the shear modulus and the Poisson coefficient. Moreover, the symbol l indicates a characteristic length which is able to simulate the size effect. This length has been discussed from a mechanical point of view in great detail in Ref. [13].

3. Numerical approximation

The numerical approach already proposed in Ref. [19], has been appropriately extended in order to incorporate an individual

microstructural parameter for any micro-beam considered for the RUC. This new feature allows to identify the separate microscale contribution of the micro-beams to the dynamic behavior, thus facilitating the optimal design of the square lattice topology. For this purpose a refined finite element has been proposed in Ref. [19].

By standard procedures, the equations of motion of the RUC assume the following matrix form:

$$\mathbf{M}_g \ddot{\mathbf{U}}_g + \mathbf{K}_g \mathbf{U}_g = \mathbf{F} \tag{13}$$

with \mathbf{M}_g and \mathbf{K}_g indicating the overall mass and stiffness matrices of the unit cell while $\mathbf{U}_g = [\mathbf{U}_1, \mathbf{U}_2, \mathbf{U}_3, \mathbf{U}_4, \mathbf{U}_5, \dots, \mathbf{U}_N]^T$ and \mathbf{F} denoting the nodal displacements and external forces vectors in the global reference system $(\mathcal{Q}, \mathbf{e}_1, \mathbf{e}_2)$, N being the number of nodes over the unit cell.

The enhanced finite element proposed in Ref. [19] is able to account for shear strains and is locking-free. These features, as it is well-known, are essential for short transient and wave propagation analysis. It is also useful to underline that the degrees of freedom $\mathbf{U}_i = [U_i, V_i, \Phi_i]^T$ of the generic i -node in the global system $(\mathbf{e}_1, \mathbf{e}_2, \mathbf{e}_3 = \mathbf{i}_3)$ are related to the corresponding degrees of freedom $\mathbf{u}_i = [u_i, v_i, \phi_i]^T$ in the local co-ordinates system $(\mathbf{i}_1, \mathbf{i}_2, \mathbf{i}_3)$ by means of an appropriate rotation due to the orientation of the finite element.

In view of analyzing the propagation of a plane elastic wave, Equation (13) can be rewritten as follows:

$$\left(-\omega^2 \mathbf{M}_g + \mathbf{K}_g \right) \mathbf{U}_g = \mathbf{F} \tag{14}$$

with ω indicating the angular frequency. The periodic boundary conditions given by Equation (4) assume the new form:

$$\mathbf{U}_1 = \mathbf{U}_3 \exp(2\pi k_1) \tag{15.1}$$

$$\mathbf{U}_2 = \mathbf{U}_4 \exp(2\pi k_2) \tag{15.2}$$

where $\mathbf{U}_1, \mathbf{U}_2, \mathbf{U}_3$ and \mathbf{U}_4 are the nodal unknowns relative to node 1 to 4, indicated in Fig. 2, which represent the connections of the RUC with the four adjacent cells and deal with the main microstructure. As a consequence, the number of degrees of freedom of the discrete model is equal to $N_{\text{dof}} = 3 \times (N - 2)$. The global displacements vector $\mathbf{U}_g = [\mathbf{U}_1, \mathbf{U}_2, \mathbf{U}_3, \mathbf{U}_4, \mathbf{U}_5, \dots, \mathbf{U}_N]^T$, in fact, can be expressed as a function of a reduced displacements vector $\mathbf{U}_r = [\mathbf{U}_3, \mathbf{U}_4, \mathbf{U}_5, \dots, \mathbf{U}_N]^T$, according to the following relationship:

$$\mathbf{U}_g = \mathbf{H} \mathbf{U}_r \tag{16}$$

where \mathbf{H} works as a transfer operator:

$$\mathbf{H} = \begin{bmatrix} c_1 \mathbf{I} & 0 & 0 & 0 & \dots & 0 \\ 0 & c_2 \mathbf{I} & 0 & 0 & \dots & 0 \\ \mathbf{I} & 0 & 0 & 0 & \dots & 0 \\ 0 & \mathbf{I} & 0 & 0 & \dots & 0 \\ 0 & 0 & \mathbf{I} & 0 & \dots & 0 \\ 0 & 0 & 0 & \ddots & \ddots & \vdots \\ \vdots & \vdots & \vdots & \ddots & \mathbf{I} & 0 \\ 0 & 0 & 0 & \dots & 0 & \mathbf{I} \end{bmatrix}, \tag{17}$$

with $\mathbf{I} = \text{diag}(1, 1, 1)$, $0 = \text{diag}(0, 0, 0)$, $c_1 = \exp(2\pi k_1)$ and $c_2 = \exp(2\pi k_2)$.

The final form of the equations of motion of the RUC are:

$$\left(-\omega^2 \mathbf{H}^T \mathbf{M}_g \mathbf{H} + \mathbf{H}^T \mathbf{K}_g \mathbf{H} \right) \mathbf{U}_r = \mathbf{H}^T \mathbf{F} \tag{18}$$

which indicates that the study of the wave transmission within the periodic square lattice material reduces to an eigenvalue problem. For fixed values of k_1 and k_2 , to be expressed in the reciprocal space $(\mathbf{b}_1, \mathbf{b}_2)$ according to Equation (5), the frequencies of the free wave propagation ($\mathbf{F} = 0$) come from the eigenvalues of the problem formulated in Equation (18). Moreover, with k_1 and k_2 lying on the boundary of the irreducible part of the first Brillouin zone, the band structure of the lattice material emerges.

4. Results and discussion

A parametric analysis has been carried out in order to identify the main factors affecting the microstructural behavior of a square 2D lattice. Geometric information and the mechanical characteristics of the reference unit cell are summarized in Table 1.

More in detail, the value of the lattice constant has been considered fixed ($a = 0.10$ mm). Three slenderness conditions have been assumed for the micro-beams. Possible auxiliary micro-beams can be present over a reduced length (l_2) along the two diagonals of the reference unit cell, according to the pattern indicated Fig. 2. II. Moreover, auxiliary micro-beams are supposed of the same material of the primary microstructure (aluminum), with the same cross-section.

Numerical analyses have been carried out with three different assumptions: a) the microscale characteristic length is zero (i.e. the

Table 5
Position and width for low frequency band gaps (1.a, 1.b, 2.a, 2.b and 2.c).

		1	2	3	4	5	6	7	8	9	10
Position		3.300	13.860	21.936	29.166	35.260	45.858	66.796	74.461	89.245	105.955
Gap	1.a	0.046	1.347	3.856	0.472	1.133	7.388	1.283	0.672	5.260	0.910
Lower band		2	6	8	9	10	12	16	18	20	22
Position		7.263	15.914	28.868	42.659	64.808	74.250	91.520	104.320	118.630	156.655
Gap	1.b	0.280	0.044	2.999	11.055	5.240	3.774	7.614	8.200	8.280	10.170
Lower band		2	4	6	8	12	14	16	18	20	26
Position		3.184	13.449	20.105	24.745	26.916	28.006	35.162	45.711	51.342	67.185
Gap	2.a	0.115	1.439	2.704	3.840	0.501	1.205	0.942	3.948	7.314	0.505
Lower band		3	10	12	13	15	16	18	22	24	28
Position		13.871	23.672	35.117	45.266	47.436	49.368	51.656	55.370	77.055	92.386
Gap	2.b	0.686	9.455	0.853	3.169	0.499	3.366	0.999	6.430	3.015	10.296
Lower band		10	12	14	18	19	21	22	24	30	32
Position		6.551	7.743	12.121	17.030	28.808	36.918	44.041	47.837	49.800	51.654
Gap	2.c	0.139	0.085	1.228	5.022	3.019	0.571	7.288	0.303	2.460	1.002
Lower band		2	3	7	8	10	12	14	16	17	18

Table 6

Position and width for low frequency band gaps (3.a, 3.b, 4.a, 4.b and 4.c).

		1	2	3	4	5	6	7	8	9	10
Position		2.857	8.280	11.555	17.961	28.563	33.799	46.465	55.418	67.474	73.009
Gap	3.a	0.111	0.136	1.255	4.842	2.050	0.162	2.845	6.006	1.592	1.699
Lower band		2	5	6	8	12	14	18	20	24	26
Position		3.929	8.603	15.246	21.933	32.922	37.802	46.771	52.732	59.765	78.084
Gap	3.b	0.040	0.637	1.494	5.063	1.592	2.106	4.650	4.031	3.723	4.523
Lower band		2	4	6	8	12	14	16	18	20	26
Position		6.664	11.465	16.660	18.132	19.258	20.364	21.083	22.083	26.502	31.221
Gap	4.a	1.319	1.082	2.434	0.167	0.462	0.887	0.551	1.176	1.354	0.429
Lower band		8	10	12	13	14	15	17	18	22	24
Position		2.627	5.868	6.658	7.827	11.467	16.948	20.694	25.786	26.357	27.088
Gap	4.b	0.207	0.976	0.605	0.538	1.086	2.990	2.465	0.175	0.556	0.906
Lower band		2	5	7	8	10	12	14	19	20	22
Position		3.491	4.343	6.180	6.735	9.296	15.239	18.721	22.359	24.429	25.520
Gap	4.c	0.111	0.133	0.352	0.759	2.839	1.544	0.005	2.966	1.174	0.760
Lower band		2	3	5	7	8	10	12	14	16	17

size effect is discarded); b) the size effect is modeled for the auxiliary beams of the RUC; c) the size effect is modeled for both primary and auxiliary beams of the RUC. It is worth remarking that if the size effect is considered, the microscale characteristic length is assumed equal to $6.58 \mu\text{m}$ [20].

The numerical simulations have been performed by means of the FE model proposed in Ref. [19]. The mesh employed has been obtained by dividing the four micro-beams of the main micro-structure, shown in Fig. 2, by 10 finite elements each one. If an auxiliary micro-beam is present, the mesh covering its axis is composed of an identical number of finite element (10). Many tests have been carried out in order to check the convergence rate and to assess the accuracy of the numerical solution.

The frequency values are identified from the eigenvalues and represented in a dimensionless form $\tilde{\omega}$ by means of:

$$\tilde{\omega} = \omega / \omega_1 \quad (19)$$

where ω_1 denotes the first bending resonance frequency of a pinned-pinned beam with the same properties given in Table 1, its length being equal to the lattice constant a :

$$\omega_1 = \frac{\pi^2}{a^2} \sqrt{\frac{EI}{\rho A}} \quad (20)$$

In Tables 2, 3 and 4 the main results concerning the lowest

natural frequencies (not dimensional) are presented. They refer to the relevant points **O**, **A** and **B** of the boundary of the irreducible part of the first Brillouin zone indicated in Fig. 3.

In the following Fig. 4 the frequency bands are plotted for the first natural modes.

In Tables 5, 6 and 7 the position and the width of the first band gaps are presented. It is also indicated the number of the lower band which bound it from below.

Many considerations are appropriate.

As an initial goal, it is relevant to make comments about the analysis concerning the configuration of the RUC when only the primary micro-beams are present (cases 1, 3 and 5). The position of the lower band gaps is mostly sensitive to the micro-scale parameter with a relevant shift (forward shift) if the size effect is considered. This influence, which can be very high (see comparison 1.a/1.b), vanishes as the stiffness of the micro-beams increases (see comparisons 3.a/3.b and 5.a/5.b).

A similar behavior concerns the configuration composed of auxiliary micro-beams in addition to the primary microstructure. From this point of view the results indicate that a partial modeling of the size effect for the auxiliary microstructure only allow to capture the major shift effects of the lower gaps when the stiffness of the micro-beams is low (see comparison 2.a/2.b/2.c).

When an auxiliary microstructure is present, flat bands also appear in the low frequency region.

Finally, the cumulative gaps are presented in Fig. 5. No effect

Table 7

Position and width for low frequency band gaps (5.a, 5.b, 6.a, 6.b and 6.c).

		1	2	3	4	5	6	7	8	9	10
Position		2.116	4.647	7.894	11.170	16.518	18.921	23.722	25.384	27.035	29.819
Gap	5.a	0.046	0.606	0.593	2.311	0.682	0.807	2.600	0.093	0.328	0.279
Lower band		2	4	6	8	12	14	16	19	20	22
Position		2.327	5.127	8.345	11.578	19.525	23.942	25.736	27.796	30.352	35.435
Gap	5.b	0.160	0.996	0.643	2.168	1.124	2.161	0.453	0.641	0.159	0.132
Lower band		2	4	6	8	14	16	17	20	22	27
Position		1.875	2.431	3.360	3.732	5.036	7.893	11.344	12.148	12.486	12.704
Gap	6.a	0.091	0.067	0.345	0.399	1.556	0.604	1.155	0.454	0.197	0.196
Lower band		2	3	5	7	8	10	14	16	17	18
Position		1.879	2.494	3.619	4.220	5.314	7.894	11.351	12.564	13.548	14.278
Gap	6.b	0.084	0.024	0.799	0.404	1.266	0.605	1.141	1.286	0.419	1.041
Lower band		2	3	5	7	8	10	14	16	18	20
Position		2.057	3.799	4.241	5.580	8.346	9.574	11.627	12.572	13.556	14.605
Gap	6.c	0.308	0.437	0.446	1.654	0.656	0.055	0.589	1.302	0.403	1.696
Lower band		2	5	7	8	10	12	14	16	18	20

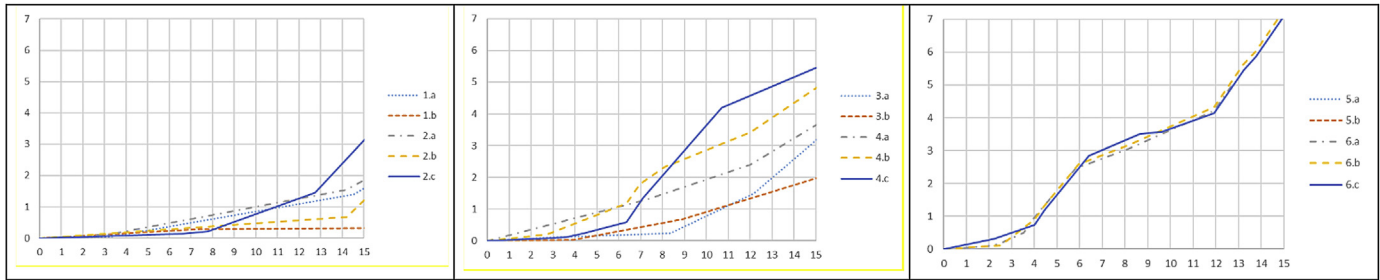


Fig. 5. Cumulative band gaps (for $\omega_1 < 15$).

depending on the topology nor on the microscale length for higher stiffness condition (cases 5 and 6) emerges. The approach based on the consideration of the micro-scale characteristic length indicates a lower cumulative gap in the low frequencies range.

5. Final comments

A microstructure-dependent scale length is introduced as an intrinsic parameter of the micro-beams of the representative unit cell. By means of an appropriate numerical approach, it is possible to detect the influence of the characteristics of the lattice at the local scale on the global dynamic behavior. Comparisons in terms of the position and width of the frequency band gaps indicate the importance of considering the microstructure-dependent scale length for both the primary and the auxiliary microstructure.

References

- [1] Gibson LJ, Ashby MF. Cellular solids: structure and properties. Cambridge: Cambridge University Press; 1997.
- [2] Maldovan M, Thomas EL. Periodic materials and interference lithography - photonic, phononic and mechanics. Wiley-Vch; 2009.
- [3] Christensen RM. Mechanics of cellular and other low-density materials. Int J Solids Struct 2000;37:93–104.
- [4] Wallach JC, Gibson LJ. Mechanical behavior of a three dimensional truss material. Int J Solids Struct 2001;38:7181–96.
- [5] Zhang YH, Fan HL, Fang DN. Constitutive relations and failure criterion of planar lattice composites. Compos Sci Technol 2008;68:3299–304.
- [6] Fan HL, Jin FN, Fang DN. Nonlinear mechanical properties of lattice truss materials. Mat Des 2009;30:511–7.
- [7] Zhou XZ, Wang YS, Zhang CZ. Effects of material parameters on elastic band gaps of two-dimensional solid phononic crystals. J Appl Phys 2009;106:14903–11.
- [8] Wang Y, Li F, Wang Y, Kishimoto K, Huang W. Tuning of band gaps for a two-dimensional piezoelectric phononic crystal with a rectangular lattice. Acta Mech Sin 2009;25:65–71. Doi: <http://dx.doi.org/10.1007/s10409-008-0191-9>.
- [9] Martinsson PG, Movchan AB. Vibrations of lattice structures and phononic band gaps. Q J Mech Appl Math 2003;56:45–64.
- [10] Phani AS, Woodhouse J, Fleck NA. Wave propagation in two-dimensional periodic lattices. J Acoust Soc Am 2006;119:1995–2005.
- [11] Zhen N, Yan Z, Wang Y. Elastic wave propagation in honeycomb materials. Chin J Theor Appl Mech 2008;40:769–75.
- [12] Gaofeng J, Zhifei S. A new seismic isolation system and its feasibility study. Earthq Eng Eng Vib 2010;75–82.
- [13] Mindlin RD. Influence of couple-stresses on stress concentrations. Exp Mech 1963;3:1–7.
- [14] Lui S, Su W. Effective couple-stress continuum model of cellular solids and size effects analysis. Int J Solids Struct 2009;46:2787–99.
- [15] Onck PR, Andrews EW, Gibson LJ. Size effects in ductile cellular solids. Part I: modelling. Int J Mech Sci 2000;34:681–99.
- [16] Andrews EW, Gioux G, Onck PR, Gibson LJ. Size effects in ductile cellular solids. Part II: experimental results. Int J Mech Sci 2000;34:701–13.
- [17] Park SK, Gao X-L. Bernoulli–Euler beam model based on a modified couple stress theory. J Micromech Microeng 2006;16:2355–9.
- [18] Ma HM, Gao X-L, Reddy JN. A microstructure-dependent Timoshenko beam model based on a modified couple stress theory. J Mech Phys Solids 2008;56(12):3379–91.
- [19] Mancusi G, Feo L. A refined finite element formulation for the microstructure-dependent analysis of two-dimensional (2D) lattice materials. Materials 2013;6(1):1–17. <http://dx.doi.org/10.3390/ma6010001>.
- [20] Shaat M. Physical and mathematical representations Of couple stress effects on micro/nanosolids. Int J Appl Mech 2015;7(1). <http://dx.doi.org/10.1142/S1758825115400128>.